LHCb-2007-067
July 30th, 2007.

LHCb VELO software alignment

Part II: the alignment of the VELO detector-halves

S. Viret, C. Parkes, M. Gersabeck

University of Glasgow

UNIVERSITY
of
GLASGOW

Abstract

The software alignment of the Vertex Locator (VELO) is a critical component of the LHCb alignment strategy. This note demonstrates a potential algorithm to perform the alignment of the VELO detector-halves. The approach described in this document, and the tools developed, are also applicable to the alignment of the other LHCb sub-systems and the global relative alignment of the sub-detectors.

Document Status Sheet

1. Document Title: A procedure for LHCb VELO online alignment			
2. Document Reference Number: LHCb-2007-67			
3. Issue	**4. Revision**	**5. Date**	**6. Reason for change**
Draft	1	February 15, 2007	First version of the box alignment note.
Draft	1	July 30, 2007	Final revision.

Contents

List of Figures

List of Tables

1 Introduction

This note describes a fast software alignment procedure to align the LHCb vertex locator (VELO) **[1]** detector-halves. This is the second stage of the VELO software alignment procedure. The first stage, the alignment of the VELO modules in their respective halves, has previously been described by the authors in **[2]** and a brief update of the results is also given here at the start of Section 4.

The alignment method for both stages is based on a non-iterative least squares fitting method which utilizes a C++ implementation[1] of the 'matrix-crushing' algorithm Millepede **[3]**. A brief overview of this procedure is presented in Section 2.

The proposed detector-halves alignment method, along with the simulation results obtained so far, are described in detail in Sections 3 and 4.

A summary, conclusions and an outline of plans for future work are given in Section 5.

2 Reminder of VELO alignment procedure

The VELO software alignment algorithm has to align the modules within each of the two VELO detector-halves and also to align the two detector-halves with respect to (w.r.t.) each other, as the two RF-boxes will be retracted and reinserted between each LHC fill. The procedure described here cannot give us information about the absolute detector positions within the LHCb frame (though we will present some results concerning alignment of the VELO w.r.t. the beam), but this link can be established using information from the position resolvers and measurements during the VELO RF-boxes insertion or from the global alignment.

The global alignment of the full VELO system with respect to the other subdetectors is not considered here. A technique is under development to perform this global alignment and is described in **[4]**. However, we note that the global alignment has less free parameters and a simpler geometry than the VELO situation, and hence could potentially also be performed using the same technique as developed here for the VELO.

The VELO alignment procedure naturally divides into two distinct parts:

1. An internal alignment of the modules within each VELO detector-half using the residuals on tracks.
2. A relative alignment of the two detector-halves w.r.t. each other using vertices (primary or beam-gas interaction) and tracks crossing both halves (overlaps).

An algorithm to perform the first step has been proposed and described in **[2]**. This algorithm has been successfully used in 2006 during two testbeam periods : the Alignment Challenge and Detector Calibration 2 and 3. Preliminary ACDC results could be found on the VELO Alignment webpage **[5]** and will be reported in a forthcoming dedicated note.

3 VELO Alignment Algorithm

3.1 Method

Clearly, track residuals within a detector-half are not sensitive to the misalignment of the whole half. Indeed the constraints applied for the internal alignment (through Lagrange multipliers) prevent any detector-half movement during this stage. Hence the alignment with standard tracks, if used on one detector-half only, will not provide any information on its position. We thus need to find other constraints, which establish a relation between the two detector-halves. There are two evident answers: **primary vertices** and **overlapping tracks**.

[1] A standalone version of this code is available from `http://ppewww.physics.gla.ac.uk/LHCb/VeloAlign/StandaloneCode.html`

3.1.1 Overlaps

Overlapping tracks are a powerful constraint for relative positioning of the two detector-halves. By overlap track we mean a normal track having at least one spacepoint (i.e. an (R, ϕ) cluster pair) in each VELO detector-half[2]. A previous study **[6]** has shown that a non-negligible amount of such tracks exist due to the small overlapping area between the two VELO detector-halves. The alignment using overlapping tracks can thus proceed by track residual minimization and hence one potentially can expect to reach a similar precision from this method for the halves as for the internal module alignment within one half **[2]**.

3.1.2 Primary Vertices

The method using primary vertices, even if less precise than the overlap technique, has some unique advantages:

- It provides information from the data on the relative position between the two detector-halves even when the VELO is open. In this case interactions between the beams and gas occuring in the VELO area could also be a useful source of tracks.
- In stable beam conditions, with the VELO closed, the constrained primary vertex fit will also provide the position of each detector-half relative to the beam. It can be assumed that the PV position in the X/Y directions is relatively constant around (x_{beam}, y_{beam}) when close to the beam spot[3].

3.1.3 The Proposed Strategy

Following from the relative advantages of the two techniques discussed above, three running scenarios for alignment algorithm are described:

- **Overlaps only** scenario : in this case the method will minimize the χ^2 given by the overlap tracks, thus finding the relative detecotr halves positions w.r.t. each other:

$$\chi^2(total) = \chi^2(overlap)$$

  .

- **PV only** : vertices can be used with or without constraining their (X,Y) position. If the transverse position is constrained then we could get the position of the halves w.r.t. the beam. If not we get the relative halves positions w.r.t. each other. This leads to the following χ^2:

$$\chi^2(total) = \chi^2(vertex)$$

- **Combining PV and overlaps** : the combination of the two methods via constraint equations is also investigated:

$$\chi^2(total) = \chi^2(overlap) + \chi^2(vertex)$$

It should be noted that 'PV only' method is the only that could be used when the VELO is in open position.

In all cases the Millepede **[3]** approach will be used. In this technique it is necessary to obtain the local and global derivatives of the system for the different cases. The derivation of these expressions is presented in the next section.

[2] Altough we don't exclude to use all the overlapping clusters in the future.

[3] This point is justified by the small spread in Z of the interaction region ($\approx \pm 5$ cm) and the relatively small crossing angle between the two beams at LHC: 285 μrad **[7]**

3.2 VELO Residuals and Global Parameters

3.2.1 General Introduction

The alignment procedure adopted here requires us to derive a linear relationship between the residuals and the alignment constants. This section is analagous to the derivation in the internal VELO alignment algorithm **[2]** of expression (30).

To define the hit coordinates in the different frames, the following notation will be used throughout this note: $\boldsymbol{r}$, $\boldsymbol{r^B}$, and $\boldsymbol{r^V}$ describe the hit coordinates in module, detector-half, and VELO frames respectively.

In the perfect case (no misalignments), transformation relations between the different frames are given by:

$$r = r^B - r_0^B = r^B - \begin{pmatrix} 0 \\ 0 \\ z_0^B \end{pmatrix} \qquad \text{and} \qquad r^B = r^V - r_0^V = r^V - \begin{pmatrix} 0 \\ 0 \\ z_0^V \end{pmatrix}, \tag{1}$$

where z_0^B and z_0^V are respectively the z position of the modules in the detector-half frame and the z position of the detector-half in the VELO frame. As a result of the constraints equations applied during the internal module alignment procedure, the relevant quantity to define is:

$$z_0^V = \frac{1}{n_{modules}} \sum_{modules} z_{modules}^V, \tag{2}$$

rather than simply putting $z_0^V = 0$.

Adding the misalignments, we get:

$$r^{new} = \Delta_R \cdot (r^{B,new} - r_0^B - \Delta_r) \qquad \text{and} \qquad r^{B,new} = \Delta_R^B \cdot (r^V - r_0^V - \Delta_r^B). \tag{3}$$

Δ_R and Δ_r represent the misalignment rotation matrix and translation vector, respectively, for the modules relative to the detector-half. Δ_R^B and Δ_r^B represent the same quantities for the transformation from the detector-half to the VELO frame. Using a superscript i to indicate the two frame transformations, these are defined as:

$$\Delta_R^i = \begin{pmatrix} 1 & \Delta_\gamma^i & \Delta_\beta^i \\ -\Delta_\gamma^i & 1 & \Delta_\alpha^i \\ -\Delta_\beta^i & -\Delta_\alpha^i & 1 \end{pmatrix} \qquad \text{and} \qquad \Delta_r^i = \begin{pmatrix} \Delta_x^i \\ \Delta_y^i \\ \Delta_z^i \end{pmatrix}, \tag{4}$$

where Δ_α^i,Δ_β^i,Δ_γ^i represent the rotations around the x,y and z axes and Δ_x^i,Δ_y^i,Δ_z^i the translations along these axes.

As the alignment of the VELO in the LHCb frame is outside the scope of this note, we use the hit position in the VELO frame, r^V, as the reference hit position. Combining the two previous expressions we end up with the global VELO tranformation relation:

$$r^{new} = \Delta_R \cdot (\Delta_R^B \cdot (r^V - r_0^V - \Delta_r^B) - r_0^B - \Delta_r), \tag{5}$$

which can be written as:

$$r^{new} = \Delta_R \Delta_R^B \cdot (r^V - r_0^V) - \Delta_R \cdot (\Delta_R^B \cdot \Delta_r^B + r_0^B + \Delta_r). \tag{6}$$

3.2.2 Overlap Tracks Case

This case is quite similar to the one treated in Ref. **[2]** for standard tracks. Since we are measuring residuals related to the hits in misaligned sensor both the position of the hit in the local frame of the sensor will change and, as the sensor has moved, the hit position in the VELO frame will also change. That is, the hit position in the VELO frame, is affected by both the module and detector-half misalignment.

Hence, we will have to determine $r^{V,new}$, i.e., the new hit position in the VELO reference frame, which will replace r^V in equation (6). To do so we use the method described in **[2]**.

As the hit belongs the sensor surface, one has:

$$r^{new} \cdot \begin{pmatrix} 0 \\ 0 \\ 1 \end{pmatrix} = 0. \tag{7}$$

Defining a straight line track in the VELO frame from:

$$\begin{array}{l} x_{track} = a \cdot z + b \\ y_{track} = c \cdot z + d \end{array}, \tag{8}$$

where a, c are the track slopes and b, d the track intercepts.

Then, since the hit belongs to the track, we have:

$$r^{V,new} = r^V + h \cdot \begin{pmatrix} a \\ c \\ 1 \end{pmatrix}, \tag{9}$$

where the h parameter quantifies the misalignment for the hit. One easily gets, at first order:

$$h = \Delta_z + \Delta_z^B + x_{hit}^V \cdot (\Delta_\beta + \Delta_\beta^B) + y_{hit}^V \cdot (\Delta_\alpha + \Delta_\alpha^B). \tag{10}$$

Replacing r^V by r, the hit co-ordinate in the module frame, in Eq. (6) one gets:

$$r^{new} = \Delta_R \Delta_R^B \cdot (r + r_0^B + h \cdot \begin{pmatrix} a \\ c \\ 1 \end{pmatrix}) - \Delta_R \cdot (\Delta_R^B \cdot \Delta_r^B + r_0^B + \Delta_r). \tag{11}$$

Replacing h by its value we finally obtain the expression for the new position of the hit in the module:

$$\left\{ \begin{array}{rcl} x^{new} & = & x - \Delta_x - \Delta_x^B + z_0^B \cdot \Delta_\beta^B + y \cdot (\Delta_\gamma + \Delta_\gamma^B) + a \cdot (\Delta_z + \Delta_z^B + x \cdot (\Delta_\beta + \Delta_\beta^B) + y \cdot (\Delta_\alpha + \Delta_\alpha^B)) \\ y^{new} & = & y - \Delta_y - \Delta_y^B + z_0^B \cdot \Delta_\alpha^B - x \cdot (\Delta_\gamma + \Delta_\gamma^B) + c \cdot (\Delta_z + \Delta_z^B + x \cdot (\Delta_\beta + \Delta_\beta^B) + y \cdot (\Delta_\alpha + \Delta_\alpha^B)) \end{array} \right. . \tag{12}$$

Defining the misalignment of the hit in the module frame as $\epsilon = (\epsilon_x, \epsilon_y)$, we obtain the required linear expression for the misalignment in terms of the global derivatives:

$$\left\{ \begin{array}{rcl} \epsilon_x & = & x^{new} - x \\ & = & -\Delta_x - \Delta_x^B + z_0^B \cdot \Delta_\beta^B + y^{new} \cdot (\Delta_\gamma + \Delta_\gamma^B) + a \cdot (\Delta_z + \Delta_z^B + x^{new} \cdot (\Delta_\beta + \Delta_\beta^B) + y^{new} \cdot (\Delta_\alpha + \Delta_\alpha^B)) \\ \epsilon_y & = & y^{new} - y \\ & = & -\Delta_y - \Delta_y^B + z_0^B \cdot \Delta_\alpha^B - x^{new} \cdot (\Delta_\gamma + \Delta_\gamma^B) + c \cdot (\Delta_z + \Delta_z^B + x^{new} \cdot (\Delta_\beta + \Delta_\beta^B) + y^{new} \cdot (\Delta_\alpha + \Delta_\alpha^B)) \end{array} \right. . \tag{13}$$

Assuming that all the module misalignments have been corrected during the internal procedure, one ends with the following relation:

$$\left\{ \begin{array}{rcl} \epsilon_x & = & -\Delta_x^B + z_0^B \cdot \Delta_\beta^B + y^{new} \cdot \Delta_\gamma^B + a \cdot (\Delta_z^B + x^{new} \cdot \Delta_\beta^B + y^{new} \cdot \Delta_\alpha^B) \\ \epsilon_y & = & -\Delta_y^B + z_0^B \cdot \Delta_\alpha^B - x^{new} \cdot \Delta_\gamma^B + c \cdot (\Delta_z^B + x^{new} \cdot \Delta_\beta^B + y^{new} \cdot \Delta_\alpha^B) \end{array} \right. . \tag{14}$$

This expression is quite similar to the one obtained in the previous note for the internal alignment. The only difference arises from the contribution of detector-half tilts $z_0^B \cdot \Delta^B_{\alpha,\beta}$. This contribution comes with a large lever arm z_0^B, thus confirming the significant effect of detector-half tilts misalignments as already observed in **[8]**.

3.2.3 Primary Vertices Case

Each vertex (v_x^V, v_y^V, v_z^V) is the origin of a certain number of tracks which would ideally satisfy the straight line track equation:

$$\left\{ \begin{array}{rcl} v_x^V & = & v_x^B = a \cdot v_z^V + b \\ v_y^V & = & v_y^B = c \cdot v_z^V + d \end{array} \right. , \tag{15}$$

where v_x^B, v_y^B represent the vertex location in the frame of one of the detector-halves, which is equivalent to the VELO frame in the absence of detector-half misalignments (at least for X and Y coordinates). a, c and b, d are, respectively, the slopes and intercepts in the detector-half frame of a track, *i.e.*the local track parameters.

In practice, the vertex position is obtained by minimizing the χ^2 contribution of all tracks, which is given by:

$$\chi^2(PV) = \sum_i \frac{(v_x^V - a^i \cdot v_z^V - b^i)^2}{\sigma^2_{v_x^V}} + \frac{(v_y^V - c^i \cdot v_z^V - d^i)^2}{\sigma^2_{v_y^V}}. \tag{16}$$

In the presence of detector-half misalignments the vertex position is seen differently in each detector-half frame. Equation (15) becomes:

$$\left\{ \begin{array}{rcl} v_x^{B,new} & = & v_x^B + \epsilon_{v_x} = a^i \cdot v_z^{B,new} + b^i \\ v_y^{B,new} & = & v_y^B + \epsilon_{v_y} = c^i \cdot v_z^{B,new} + d^i \end{array} \right. , \tag{17}$$

where $v_x^{B,new}, v_y^{B,new}$ denote the PV coordinates in the misaligned detector-half frame and $\epsilon_{v_x}, \epsilon_{v_y}$ the vertex misalignment. Assuming the internal alignment has already been performed, a point is transformed from the module frame to the detector-half frame by:

$$r^{B,new} = \Delta_R^B \cdot (r^B - \Delta_r^B). \tag{18}$$

Hence, PV coordinates in a misaligned detector-half frame are related to the true position in the detector-half frame via the relation:

$$\left\{ \begin{array}{rcl} v_x^{B,new} & = & v_x^B - \Delta_x^B - v_y^B \cdot \Delta_\gamma^B + v_z^B \cdot \Delta_\beta^B \\ v_y^{B,new} & = & v_y^B - \Delta_y^B + v_x^B \cdot \Delta_\gamma^B + v_z^B \cdot \Delta_\alpha^B \\ v_z^{B,new} & = & v_z^B - \Delta_z^B - v_y^B \cdot \Delta_\alpha^B - v_x^B \cdot \Delta_\beta^B \end{array} \right. . \tag{19}$$

Note that there is a significant difference here between the overlap track case and the primary vertex case. In the overlap track case, the hits move in the VELO frame as the detector-halves are misaligned. However, in the vertex case the PV remains fixed in the VELO frame as the detector-halves are misaligned, that is :

$$\left\{ \begin{array}{rcl} v_x^{V,new} & = & v_x^V \\ v_y^{V,new} & = & v_y^V \\ v_z^{V,new} & = & v_z^V \end{array} \right. . \tag{20}$$

We now have all the elements in required to obtain a relation between the local (track and vertex) parameters and the global (misalignment) parameters. Substituting equation (19) in equation (17) one obtains:

$$\left\{ \begin{array}{rcl} v_x^B - \Delta_x^B - v_y^B \cdot \Delta_\gamma^B + v_z^B \cdot \Delta_\beta^B & = & a \cdot (v_z^B - \Delta_z^B - v_y^B \cdot \Delta_\alpha^B - v_x^B \cdot \Delta_\beta^B) + b \\ v_y^B - \Delta_y^B + v_x^B \cdot \Delta_\gamma^B + v_z^B \cdot \Delta_\alpha^B & = & c \cdot (v_z^B - \Delta_z^B - v_y^B \cdot \Delta_\alpha^B - v_x^B \cdot \Delta_\beta^B) + d \end{array} \right. , \tag{21}$$

which can be rewritten as:

$$\begin{cases} b &= v_x^B - a \cdot v_z^B - \Delta_x^B + a \cdot \Delta_z^B + a \cdot v_y^B \cdot \Delta_\alpha^B + (v_z^B + a \cdot v_x^B) \cdot \Delta_\beta^B - v_y^B \cdot \Delta_\gamma^B \\ d &= v_y^B - c \cdot v_z^B - \Delta_y^B + c \cdot \Delta_z^B + (v_z^B + c \cdot v_y^B) \cdot \Delta_\alpha^B + c \cdot v_x^B \cdot \Delta_\beta^B + v_x^B \cdot \Delta_\gamma^B \end{cases} . \quad (22)$$

Now, given that the vertex is close to the beam (*i.e.*v_x^B and v_y^B are < 1 mm) [4] we obtain at first order:

$$\begin{cases} b &= v_x^B - a \cdot v_z^B - \Delta_x^B + a \cdot \Delta_z^B + v_z^B \cdot \Delta_\beta^B \\ d &= v_y^B - c \cdot v_z^B - \Delta_y^B + c \cdot \Delta_z^B + v_z^B \cdot \Delta_\alpha^B \end{cases} , \quad (23)$$

which is the equation we will use in Millepede in order to fit both vertices and detector-half misalignments.

The global parameters we are sensitive to in the detector-half alignment are $\Delta_{x,y,z}^B$ and $\Delta_{\alpha,\beta}^B$. The fact that we are not sensitive to Δ_γ^B is not really a surprise: the interaction region has a very small width in X and Y, thus providing a weak lever arm for any Z rotational constraint.

Note that each of these expressions contains a large non-linear contribution: respectively $v_z^B \cdot \Delta_\beta^B$ and $v_z^B \cdot \Delta_\alpha^B$. An iterative procedure is used to cope with this problem. A rough estimate[5] of v_z^B is used for the first iteration and then is replaced by the one obtained from the local Millepede fit (the same method is used for non-linear weak degrees of freedom of the internal alignment step).

In the case of performing the relative alignment of the detector-halves, one detector-half is fixed and the position of the other half is determined. As we are not sensitive to the z-axis rotation, there are five alignment parameters to determine. If we use only primary vertices coming from the interaction region, we could assume that they are all coming, in average, from the same transverse position: $(v_x, v_y) = (x_{beam}, y_{beam})$. Adding this constraint to the vertex fit, one could get the position of both detector-halves w.r.t. the beam, thus leading to ten global parameters.

3.2.4 Constraining the detector-half alignment within Millepede

As discussed in section 3.1.3 there are different possible scenarios for the VELO halves alignment, depending on the VELO configuration: open or closed.

The open VELO alignment will be done using only vertices coming from beam gas events or from collisions. In the first case only the relative position of one detector-half w.r.t. the other will accessible. The constraint to apply then is straightforward: one has just to fix one detector-half. When the VELO is closed and the beam stable one will also have the possibility to get the detector-halves positions w.r.t the beam.

The degrees of freedom accessible to us in this case are summarized in Table 1.

Method	**Accessible degrees of freedom**
Overlaps only (VELO closed)	Δ_x^B, Δ_y^B, Δ_z^B, Δ_α^B, Δ_β^B, Δ_γ^B
PV only (always)	Δ_x^B, Δ_y^B, Δ_z^B, Δ_α^B, Δ_β^B
PV only (VELO closed)	$\Delta_x^{B^{r,l}}$, $\Delta_y^{B^{r,l}}$, $\Delta_z^{B^{r,l}}$, $\Delta_\alpha^{B^{r,l}}$, $\Delta_\beta^{B^{r,l}}$

Table 1 *Available degrees of freedom of the detector-half alignment.*

The Δ^{B^r} and Δ^{B^l} parameters denote the right and left halves (respectively C and A side) misalignments w.r.t. the beam respectively. The Δ^B parameters denote the relative alignment of the A and C halves determined from overlap tracks. Since the relative offset of the detector-halves determined

[4] preliminary investigations of beam gas interactions have already been started and the approximation still appears to be sufficiently valid.

[5] This estimate is obtained via a classic PV fit method.

from the PV and the overlap tracks must be the same, these parameters are related by the following set of constraint equations:

$$\Delta_i^B = \Delta_i^{B^r} - \Delta_i^{B^l} \qquad \text{with} \qquad i = (x, y, z, \alpha, \beta). \tag{24}$$

These equations are straightforward to implement into the Millepede framework.

4 Results

4.1 Principle of the study

The results of the internal alignment algorithm have been evaluated using simulation events and are reported in this section.

200 samples of 25000 events each have been produced and propagated through the LHCb simulation packages. Each sample had a different set of alignment constants which were introduced into the LHCb geometry using the LHCb Geometry Framework described in **[9]**.

The misalignment values have been randomly choosen within a Gaussian distribution centered on 0 and with the resolution σ_{scale}. The different scales are summarized in Table 4.1, and are inspired by the study in **[8]**. The rotations and translations of both the modules and the detector-halves have been considered.

Component	**Degree of freedom**	σ_{scale}
Module	Δ_x, Δ_y, Δ_z	30 μm
Module	Δ_α, Δ_β, Δ_γ	2 mrad
Detector-half	$\Delta_x^{B^{r,l}}$, $\Delta_y^{B^{r,l}}$, $\Delta_z^{B^{r,l}}$	100 μm
Detector-half	$\Delta_\alpha^{B^{r,l}}$, $\Delta_\beta^{B^{r,l}}$, $\Delta_\gamma^{B^{r,l}}$	1 mrad

Table 2 *Misalignment scales for detector-half alignment studies.*

Each sample comprises a mixture of 5000 minimum bias events ($\approx$ 100,000 tracks) plus 20000 'pseudo-halo' tracks. As an LHCb simulation of beam halo tracks is not currently available these were generated by producing high energy particles in GEANT4 at small angles to the beam axis and uniformly distributed over the silicon sensor surface using the 'particle gun' option. These tracks are denoted 'pseudo-halo' tracks below.

Both of the VELO pattern recognition algorithms were used: the standard VELO pattern recognition algorithm **[10]** was run first and then additional tracks were found using generic pattern recognition algorithm **[11]**. The generic pattern recognition algorithm has been particularly tuned for the open VELO case. This algorithm is also required as the standard pattern recognition algorithm does not currently select overlap tracks.

4.2 Internal Alignment Results

A brief reminder and update of the results on the internal alignment of the modules inside each VELO detector-half is given in this section. This update demonstrates the improvement obtained using a mixture of minimum bias and pseudo-halo tracks over the use of minimum bias tracks alone presented in **[2]**. Unlike the previous study, the alignment is now run over the full set of VELO modules in each detector-half.

4.2.1 Sensitivity to Major Degrees of Freedom

The internal alignment of the modules is primarily sensitive to translations of the modules in the x and y directions and rotations around the z-axis (Δ_γ). Results on the alignment of all modules in a detector-half are obtained with minimum bias event tracks alone and with a mixture of minimum bias and pseudo-halo tracks and are presented on Figs. 1 & 2 respectively. They clearly demonstrate the improvement obtained if a complementary set of tracks is used. In particular, the systematic effects observed for backward modules (0 to 3), due to the fact that we are using only tracks coming from the interaction region, disappear when the pseudo-halo tracks are added. This difference is shown quantitatively on Figs. 3 & 4 where the fits of the alignment constants after the alignment procedure are shown in both cases. The resolution on the X and Y translation alignment parameters improves from 5.0 μm to 1.3 μm, whereas the resolution on rotation around the z-axis goes from 0.29 mrad to 0.12 mrad [6].

4.2.2 Sensitivity to Weak Degrees of Freedom

In addition to constraining the major degrees of freedom some sensitivity is also obtained to the other degrees of freedom Δ_α, Δ_β, and Δ_z. This sensitivity is primarily for the modules which are close to the interaction region, i.e. where track slopes are larger, as can be seen in Figure 5. Restricting the study to these stations (1 to 14), one obtains a reasonable sensitivty to Δ_z (28 μm) and a fair sensitivity to Δ_α and Δ_β (0.8 mrad and 1.1 mrad respectively), as shown on Fig. 6.

4.3 Detector-half Alignment Results

In all the results presented below the full alignment procedure has been applied: the internal module alignment is performed followed by the detector-half alignment[7]. The tracks are refitted after the internal alignment procedure in order to update their parameters. Before feeding Millepede, a preliminary vertex fit is made in order to select only the good PV candidates.

This note presents only the results of the alignment for a closed VELO. As said previously, we can access two types of information in this case: the position of the detector-halves w.r.t. each other (using overlaping tracks only or primary vertices only); and the position of the detector-halves w.r.t. the beam (using primary vertices combined or not with overlap tracks information). Below we present a comparison of the results obtained with the different possibilities.

The results presented have been obtained with relatively low statistics: about 300 overlap tracks and 1500 vertices. Thus, there is still significant possibility for improvement.

4.3.1 Case 1 : Overlaps only

Figure 7 shows the results obtained when running on overlap tracks, fixing one detector-half, for the major detector-half degrees of freedom (Δ_x^B, Δ_y^B, Δ_α^B and Δ_β^B). Top plots show the correlations between the generated misalignments and the reconstructed ones, for offsets (left), and tilts (right). Bottom plots show the corresponding resolution. As we will see later, results with this technique are as expected much more accurate than the PV method. Resolutions obtained are:

- **Detector-half position w.r.t. each other (from overlaps only)** : 17 μm for x and y translations, 61 μrad for x and y tilts.

[6] The initial X and Y translation resolution is worse than that reported in **[2]** as all modules are considered here not just those in the forward direction. The z-axis rotation resolution is better than that previously reported due to a bug fix in the pattern recognition code

[7] Though the two steps could be processed independently.

4.3.2 Case 2 : PV only

As said previously, the information coming from primary vertices could be used into two different ways: either to determine the relative position of the two detector-halves by fixing one detector-half, or to obtain the position of each detector-half with respect to the beam by constraining the vertex transverse position.

All the results presented here have been obtained with the closed-VELO configuration. However, they can be easily extrapolated to the open-VELO situation. Indeed, the VELO generic tracking is not affected by the VELO detector-halves position **[11]**, and one should just expect a degradation of the alignment constants resolution due to a worse vertex position resolution (as shown in **[11]** this degradation is due to the fact that one gets less tracks per vertices in the open configuration).

Figure 8 shows the results obtained when running with one detector-half fixed, for the major detector-half degrees of freedom (Δ_x^B, Δ_y^B, Δ_α^B and Δ_β^B). Top plots show the correlations between the generated misalignments and the reconstructed ones, for offsets (left), and tilts (right). Bottom plots show the corresponding resolution.

Figure 9 shows the same results, but now with the vertex transverse position constrained. Degrees of freedom represented are now $\Delta_x^{B^{r,l}}$, $\Delta_y^{B^{r,l}}$, $\Delta_\alpha^{B^{r,l}}$ and $\Delta_\beta^{B^{r,l}}$. A red dotted line on each of the top plots shows that the results in this case doesn't lie on the diagonal as expected. A slight bias appears, particularly for large misalignments (this explain the outliers seen on the resolution plots of Fig. 9). This bias comes from the fact that for large misalignments relation (23) becomes less accurate, in particular if we consider that all the vertices are coming from the same (X,Y) position.

Finally, the best resolutions obtained if one uses only the PV information are:

- **Detector-half position w.r.t. each other (from PV only)** : 35 μm for x and y translations, 166 μrad for x and y tilts.
- **Detector-half position w.r.t. the beam (from PV only)** : 36 μm for x and y translations, 190 μrad for x and y tilts.

One should also notice that the chi-square of the fit is slightly worse in the 'position-constrained' case, due to the bias cited before. This bias is indeed much smaller in the unconstrained case.

4.3.3 Case 3 : Combining PV and overlaps

As said previously one can also try to run in parallel the PV and overlap techniques in order to improve the resolution, using the constraint equations presented in Section 3.2.4.

Results obtained in this case are shown on Fig. 10. In particular, the resolution plots show that using the constraints not only improves the resolution of the absolute detector-half positions w.r.t. the beam ($\mathcal{O}(10\%)$ improvment), but also provides a good correction for all the parameters (χ^2 of the distributions is much better).

The resolutions obtained, i.e. the ones using the combined method, are:

- **Detector-half position w.r.t. the beam (from PV combined with overlaps)** : 33 μm for x and y translations, 173 μrad for x and y tilts.

The relative detector-half position resolutions stay unchanged, as they are obtained with the overlaps which provide a much stronger constraint and thus don't benefit from the PV addition.

Once again, these results have been obtained with low statistics, and a clear improvment could be expected with more events. For example, a suitable aim might be to select $\mathcal{O}(1000)$ overlap tracks in LHCb and combine with, say, $\mathcal{O}(5000)$ primary vertex events.

4.3.4 Results with reduced detector-half tilts

The detector-half tilts chosen in this study are large, 1 mrad may be a more reasonable assumption for the mechanical accuracy with which the detector-half will be positioned. In this case, we observe a slightly better resolution for all the parameters, thus giving the best results in all cases:

- **Detector-half position w.r.t. each other (from overlaps only)** : 12 μm for x and y translations, 36 μrad for x and y tilts.
- **Detector-half position w.r.t. each other (from PV only)** : 28 μm for x and y translations, 108 μrad for x and y tilts.
- **Detector-half position w.r.t. the beam (from PV combined with overlaps)** : 18 μm for x and y translations, 103 μrad for x and y tilts.
- **Detector-half position w.r.t. the beam (from PV only)** : 24 μm for x and y translations, 121 μrad for x and y tilts.

In the case where the detector-halves are aligned w.r.t. the beam, the difference between the combined and uncombined methods becomes slightly larger, most markedly for the rotation parameters (tilts).

In the combined case, the resolutions obtained for the translation parameters are well within the trigger requirements. The resolution obtained for tilts w.r.t. the beam are a little worse than may be hoped for but are still within the requirements. These resolution would improve somewhat with more PVs than used in this study. Moreover, apart from increasing the statistics, one could also select PV at larger Z. This would provide a better sensitivity to the tilts by increasing the lever arm.

4.3.5 Sensitivity to weak degrees of freedom

As for the internal alignment, some degrees of freedom are more difficult to constrain. In the detector-half alignment case, these weak degrees are the ones related to the Z-axis: rotation around and translation along. However, one could get some sensitivity to both of them by using the different methods presented.

Relative rotation around Z between the two detector-halves could be constrained using the overlap tracks. Quantitatively, this leads us to the sensitivity plot shown on Fig. 11. The upper plot shows a clear correlation between the generated and the reconstructed Z tilt. The bottom plot shows that the resolution is a factor of 4 better than the introduced misalignment scale. This value could be slightly improved, if necessary, with more tracks.

For translation along Z vertices provide a much more important constraint than overlap tracks. Indeed, fitting a vertex independently in the two detector-halves, and comparing the two Z positions obtained, one gets a fairly precise view of the relative Z distance between the 2 detector-halves. However, in order not to bias the Z position of the fitted vertex, one should not constrain its transverse position. Thus the best constraint on the Z translation between the two detector-halves is obtained in 'open-VELO' mode. In this case, one gets the result shown on Fig. 12. As expected, the resolution is slightly worse than for the X and Y parameters (40 μm), but it is still relatively accurate and well within LHCb requirements.

5 Conclusion

A fast alignment method for the LHCb vertex locator has been developed. This procedure performs the alignment in two steps. First, an internal alignment of VELO modules within each RF-box, using track residuals. Then, since the detector-halves are moved between each LHC fill, a second step is required in order to align the detector-halves w.r.t. to each other, thus providing a fully internally aligned VELO. This step, which is based on the utilization of tracks that pass through both VELO-halves and on primary vertices, has been described in detail and results presented in this note. A

method for performing the relative alignment of the open VELO has also been proposed in this note but the results presented here are only for a closed VELO situation.

The proposed VELO alignment strategy utilises the Millepede program, which enables the alignment to be performed in only one pass; this is to be compared with classic minimization methods which require many iterations to provide their result.

An update concerning the internal alignment results described in **[2]** has been presented. This shows that if a set of tracks (halo, beam gas,...) is used which is complementary to the standard physics tracks the VELO alignment results can be significantly improved. A 1.3 μm precision could be expected on the relevant translational degrees of freedom (i.e. along x and y axes), and a 0.1 mrad accuracy on the rotation around the z-axis. This is an important advance over the previous study as it shows that using a mixture of tracks an alignment of the VELO can be obtained at a precision that would not limit the performance of the detector. Future work will be undertaken to attempt to select the required tracks in the LHCb trigger.

The results of the detector-half alignment procedure obtained show that the tracks that overlap between the two VELO detector-halves provide, as expected, a very strong constraint. With only a few hundred tracks and detector-half tilts lower than 1 mrad, accuracies of 12 μm for x and y translations, and 36 μrad for x and y tilts, are obtained. These results are well within the system requirements.

The primary vertex method is by definition less constraining than the overlap one. However, it's the only method that could be used when the VELO is open. With only 1500 vertices and detector-half tilts of lower than 1 mrad, accuracies of 28 μm for x and y translations, and 108 μrad for x and y tilts, are obtained. These results are expected to be comparable, tough a little worse, with an open VELO (we have less tracks per vertices so that we loose some precision).

Apart from the fact that it could be run when VELO is open, an interesting property of the alignment with primary vertices is that one could use it to align the detector-halves w.r.t. the beam. The idea proposed in this note is to combine in this case the alignment with PVs with the alignment with overlaps through the use of contraints. As expected the constraints provide a significant improvement to the PV method results, if this one is used to get the detector-halves position w.r.t. the beam. Indeed, restricting ourselves to detector-halves tilts lower than 1 mrad, one get accuracies of 17 μm for x and y translations, and 103 μrad for x and y detector-halves tilts. The results obtained without constraints were 24 μm and 121 μrad respectively. This method could potentially be of interest if external information on the position of the VELO halves in the global frame is required.

In conclusion this note has demonstrated the feasibility of performing the second critical stage of the VELO software alignment. The results obtained on the detector-halves alignment fulfill the requirements of LHCb. The CPU requirements of this algorithm are suitable for operation in the LHCb environment. This note completes the initial strategy for the LHCb VELO software alignment algorithm and the group is now considering the issues related to its integration within LHCb running conditions.

6 References

[1] LHCb Collaboration - *LHCb VELO technical design report* - LHCb TDR 5 - CERN-LHCC 2001-010

[2] S. Viret, C. Parkes, D. Petrie - *LHCb VELO software alignment: Part I* - LHCb-2005-101

[3] V. Blobel and C. Kleinwort - *A new method for the high-precision alignment of track detectors* - hep-ex/0208021

[4] W. Baldini *et al.* - *LHCb Alignment Strategy* - LHCb-2006-035

[5] S. Viret, M. Gersabeck, C. Parkes - *VELO alignment webpage* - `http://ppewww.ph.gla.ac.uk/LHCb/VeloAlign/`

[6] S. Viret - *Overlapping areas in the Vertex Locator* - LHCb-2007-061

[7] LHCb Collaboration - *LHCb reoptimized detector technical design report* - LHCb TDR 9 - CERN-LHCC 2003-030

[8] D. Petrie, C. Parkes, S. Viret - *Study of the impact of VELO misalignments on the LHCb tracking and L1 trigger performance* - LHCb-2005-056

[9] J. Palacios - *LHCb Geometry Framework* - `https://uimon.cern.ch/twiki/bin/view/LHCb/GeometryFramework`

[10] D. Hutchcroft - *VELO Pattern Recognition* - LHCb-2007-013

[11] T. Lastovicka - *VELO Generic Pattern Recognition* - LHCb-2007-002 - *to appear soon*

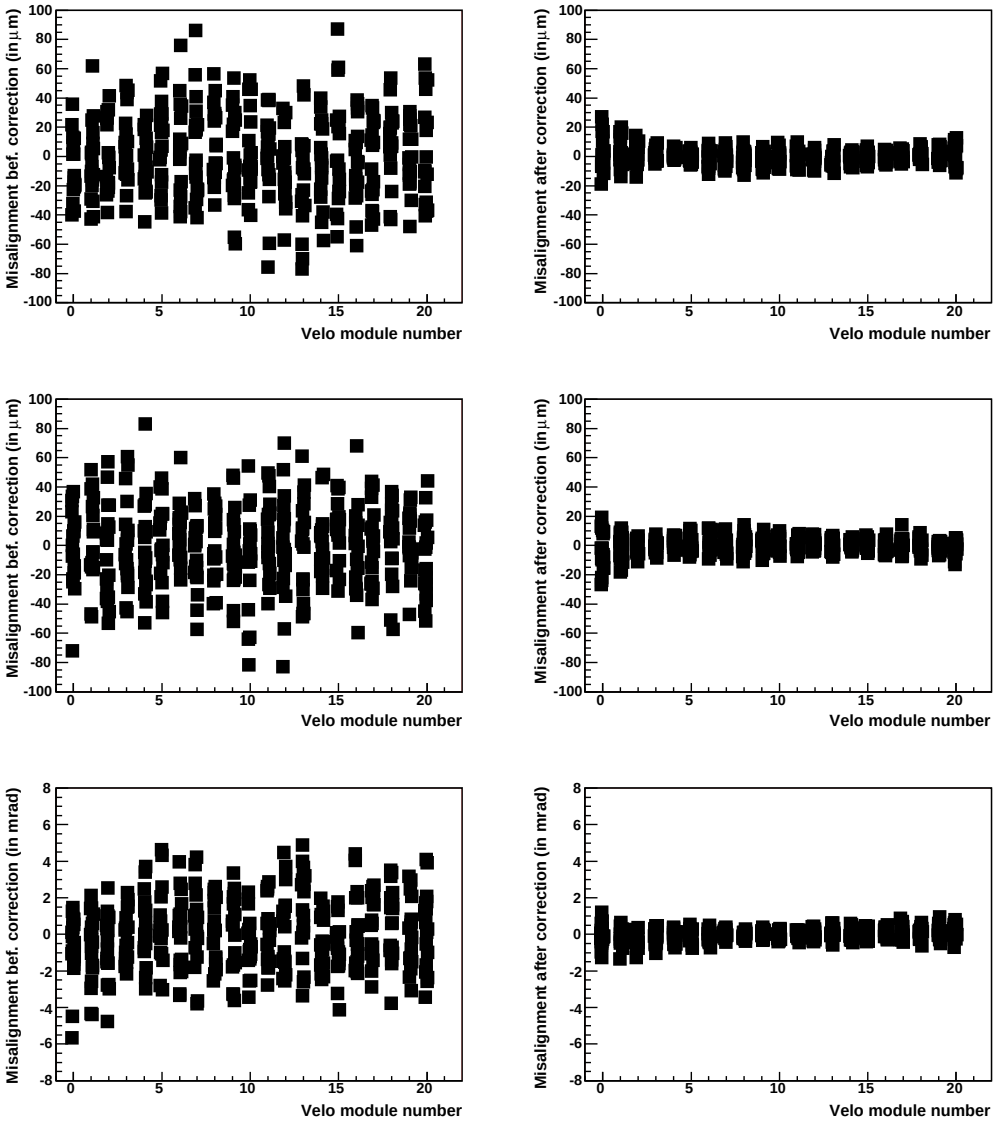

Figure 1 *Results of performing an internal alignment of VELO modules using only tracks from minimum bias events. For each station each point corresponds to a different set of misalignments. Left plots shows the misalignment constants for X translations (top), Y translations (middle), and Z rotations (bottom) before alignment. Right plots show the same constants after correction.*

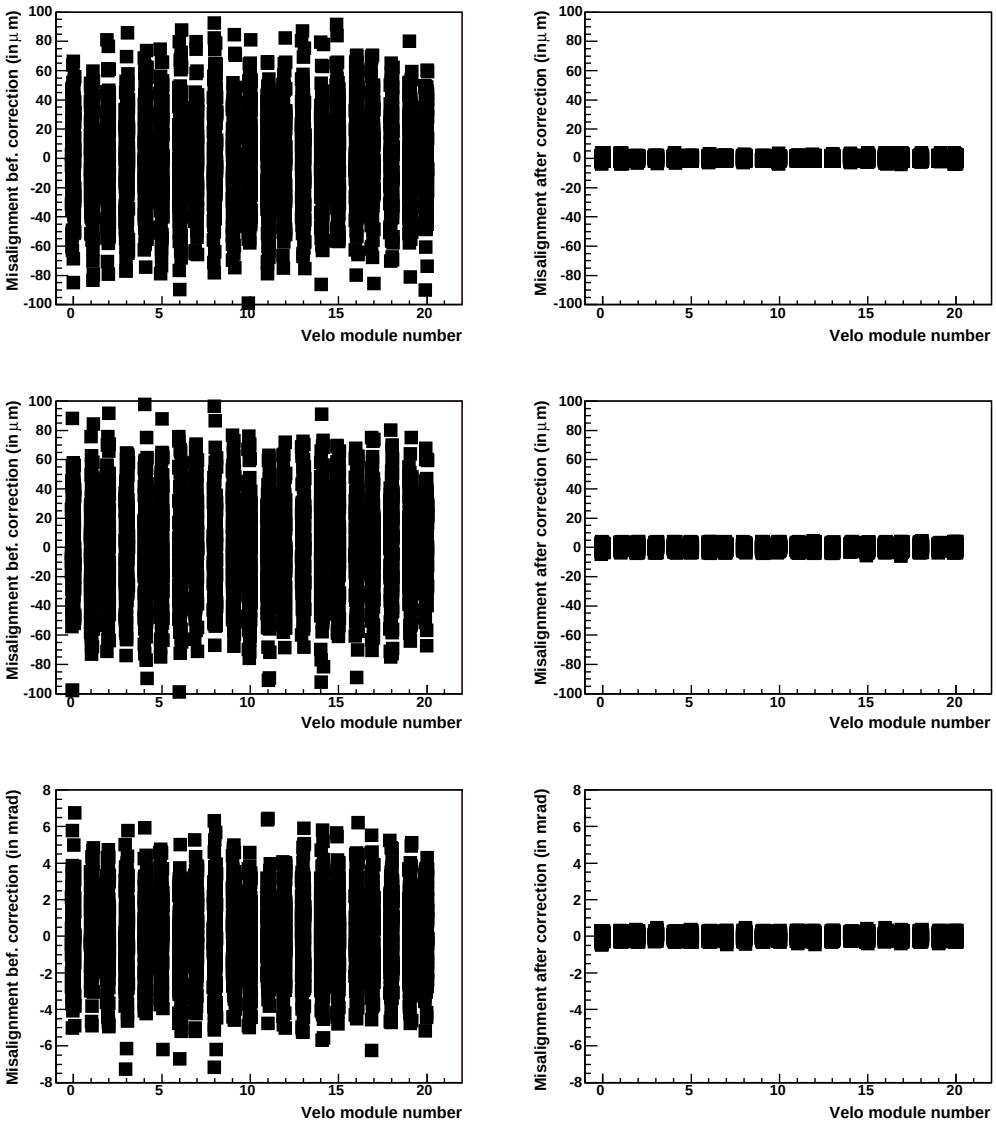

Figure 2 *Results of performing an internal alignment of VELO modules using tracks from minimum bias events and 'pseudo-halo' tracks. For each station each point corresponds to a different set of misalignments. Left plots show the misalignment constants for X translations (top), Y translations (middle), and Z rotations (bottom) before alignment. Right plots show the same constants after correction.*

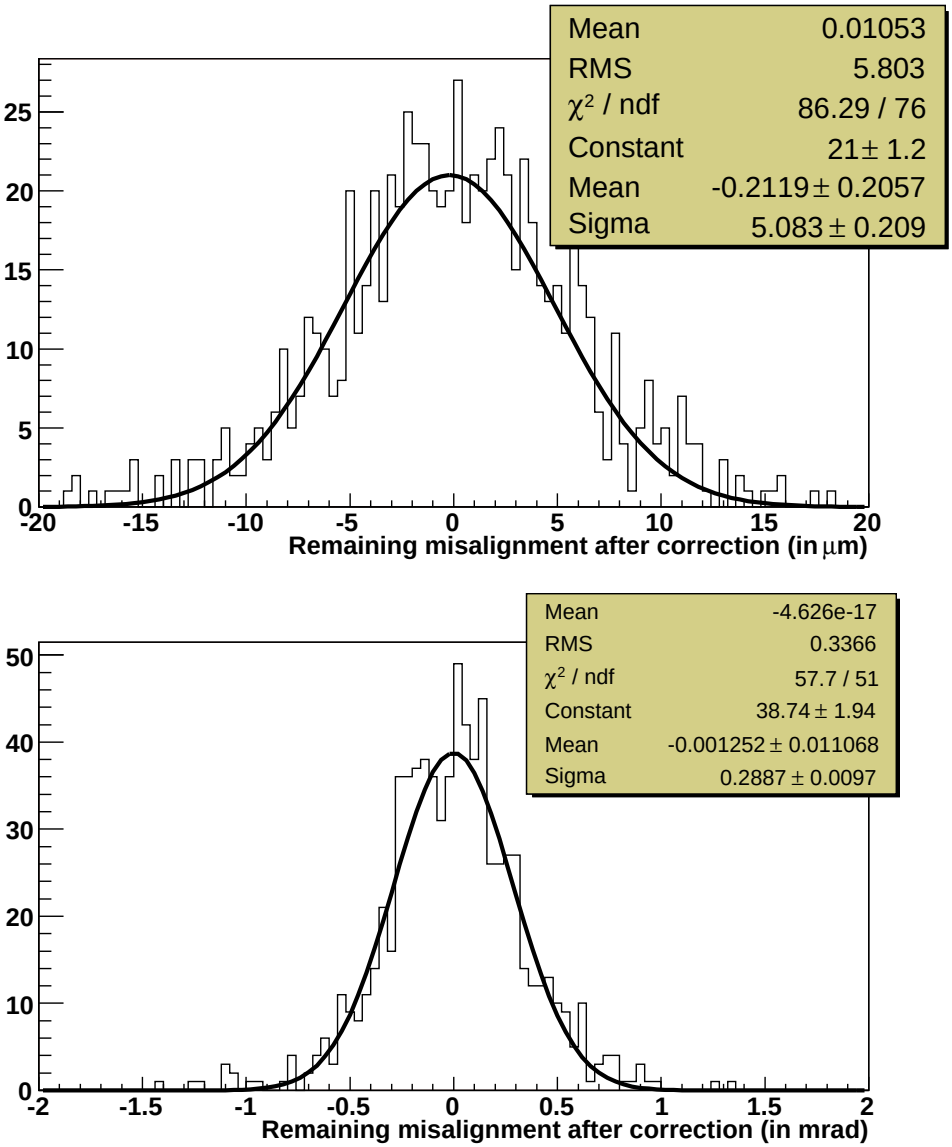

Figure 3 *Resolution on the corrected misalignment constants for the internal VELO module alignment using only tracks from minimum bias events. Results from 200 sets of misalignments are shown. Top plot shows the result for the X and Y translations (in μm), bottom plot shows the result for Z rotation (in mrad).*

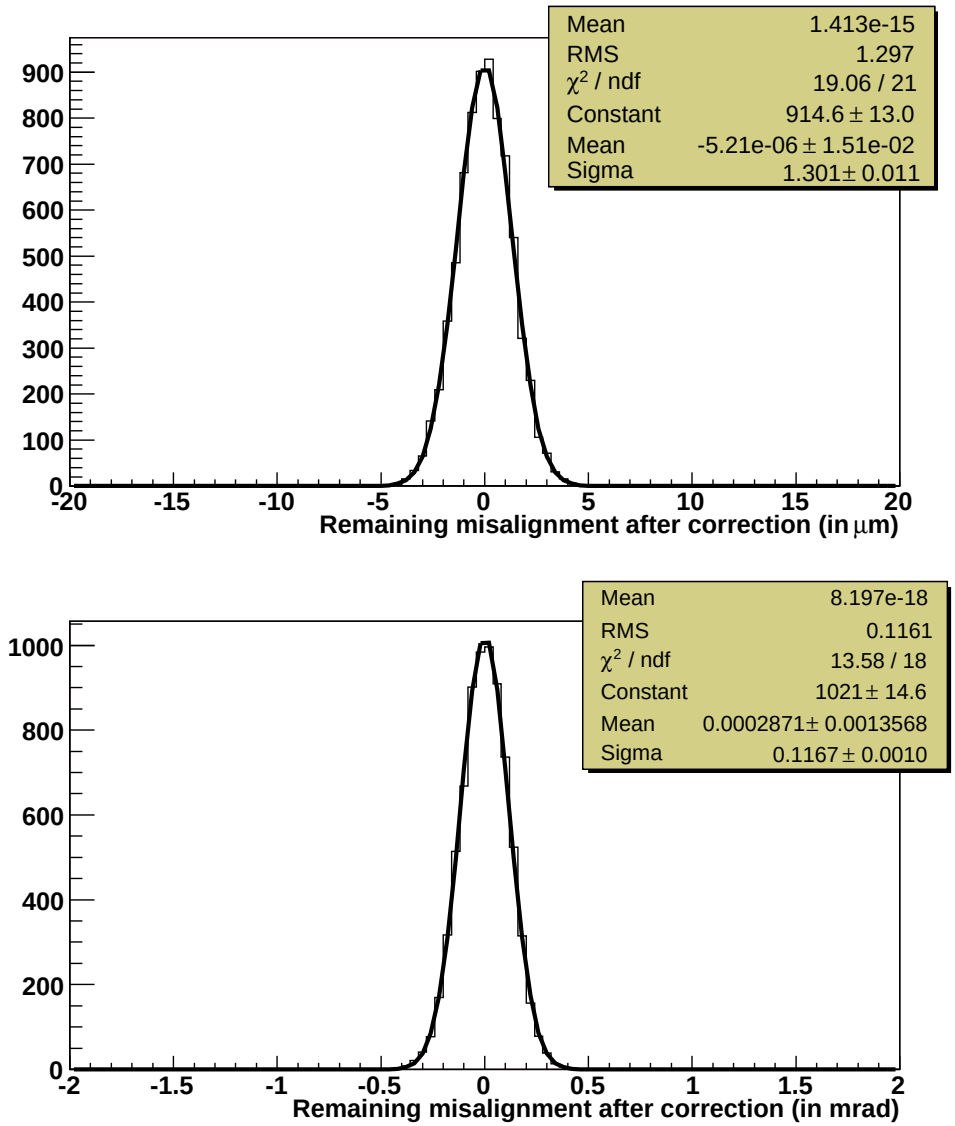

Figure 4 *Resolution on the corrected misalignment constants for the internal VELO module alignment using tracks from minimum bias events and 'pseudo-halo' tracks. Results from 200 sets of misalignments are shown. Top plot shows the result for the X and Y translations (in μm), bottom plot shows the result for Z rotation (in mrad).*

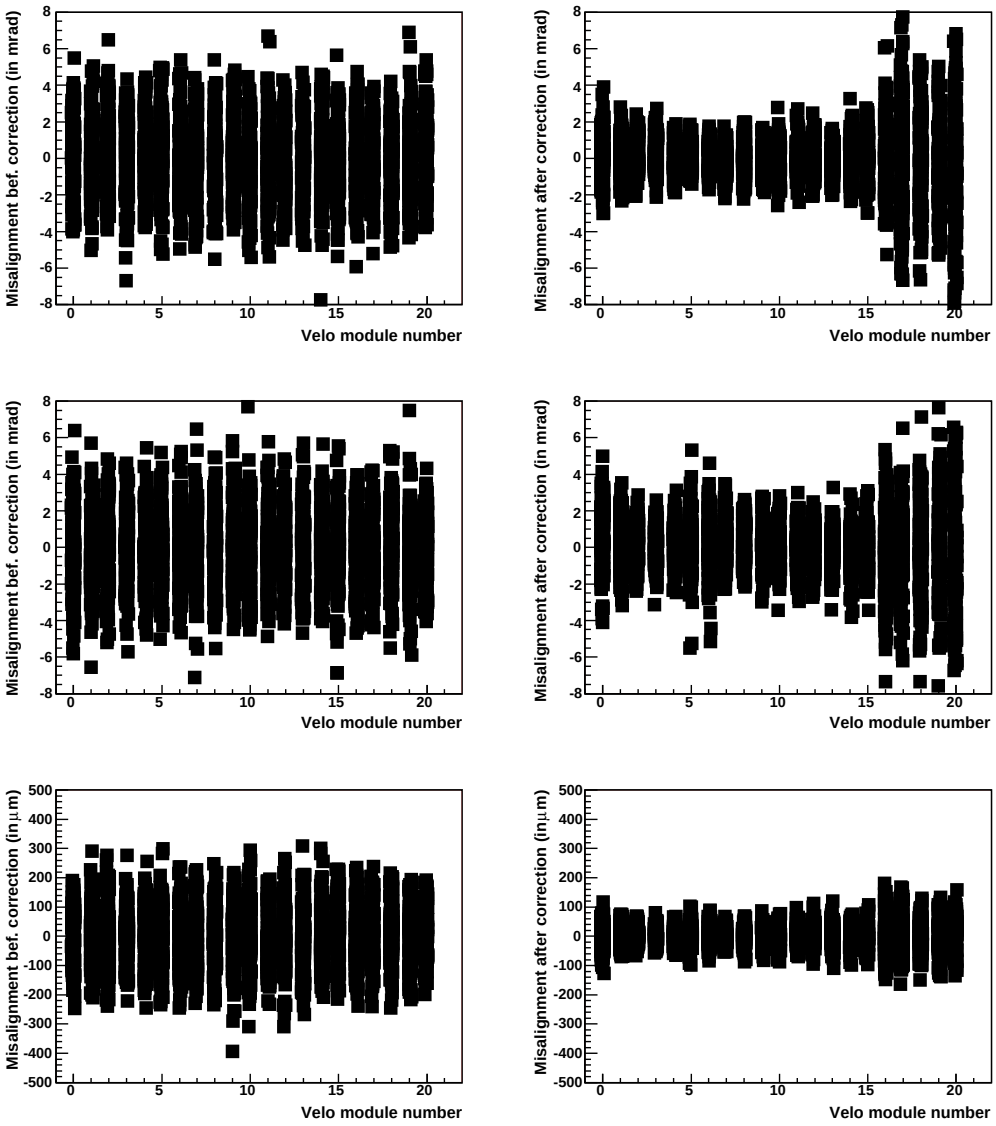

Figure 5 *Results of performing an internal alignment of VELO modules using tracks from minimum bias events and 'pseudo-halo' tracks. For each station each point corresponds to a different set of misalignments. Left plots shows the misalignments constants for X rotations (top), Y rotations (middle), and Z translations (bottom) before alignment. Right plots show the same constants after correction.*

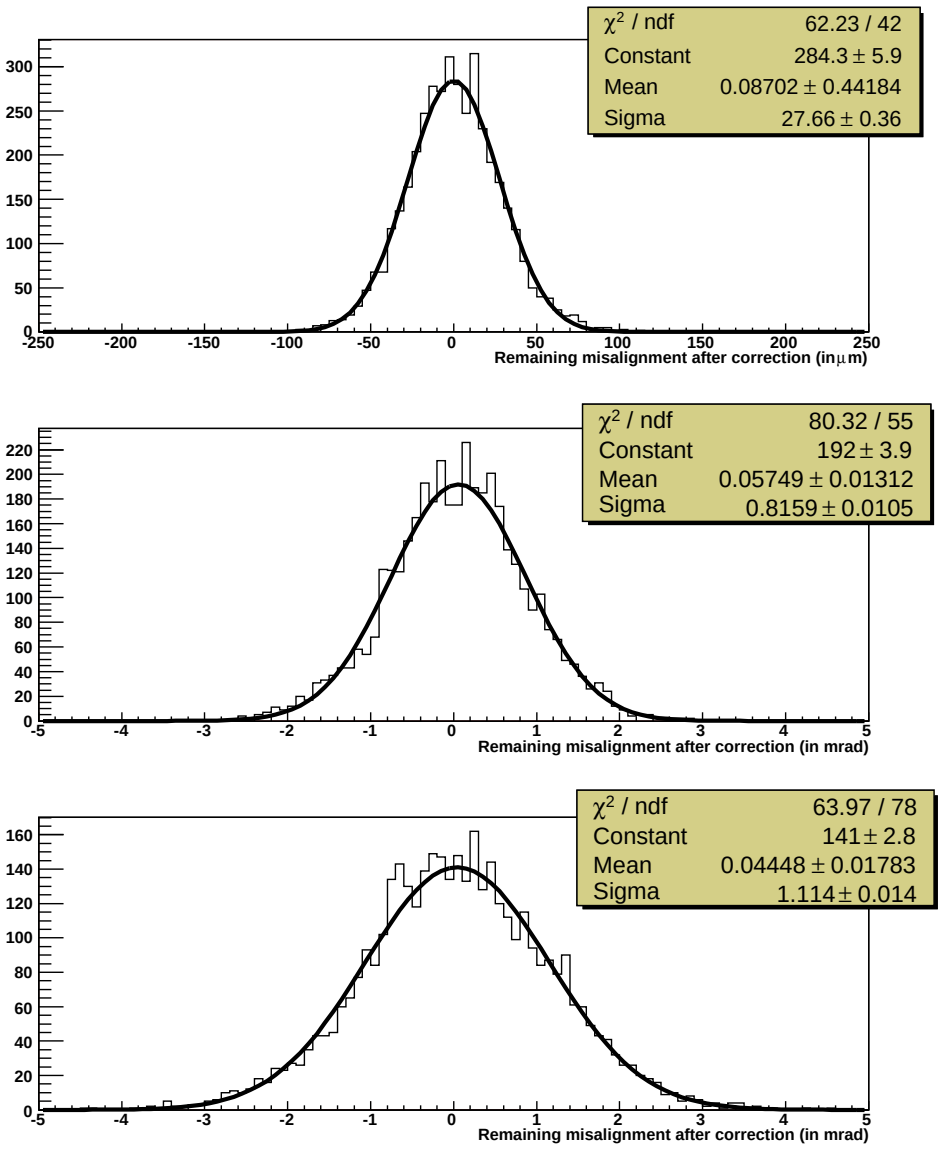

Figure 6 *Resolution on the corrected misalignment constants for the internal VELO module alignment using tracks from minimum bias events and 'pseudo-halo' tracks. Results from 200 sets of misalignments are shown. Top plot shows the result for the Z translations (in μm), the middle plot shows the result for X rotations (in mrad) and the bottom plot shows Y rotations (in mrad).*

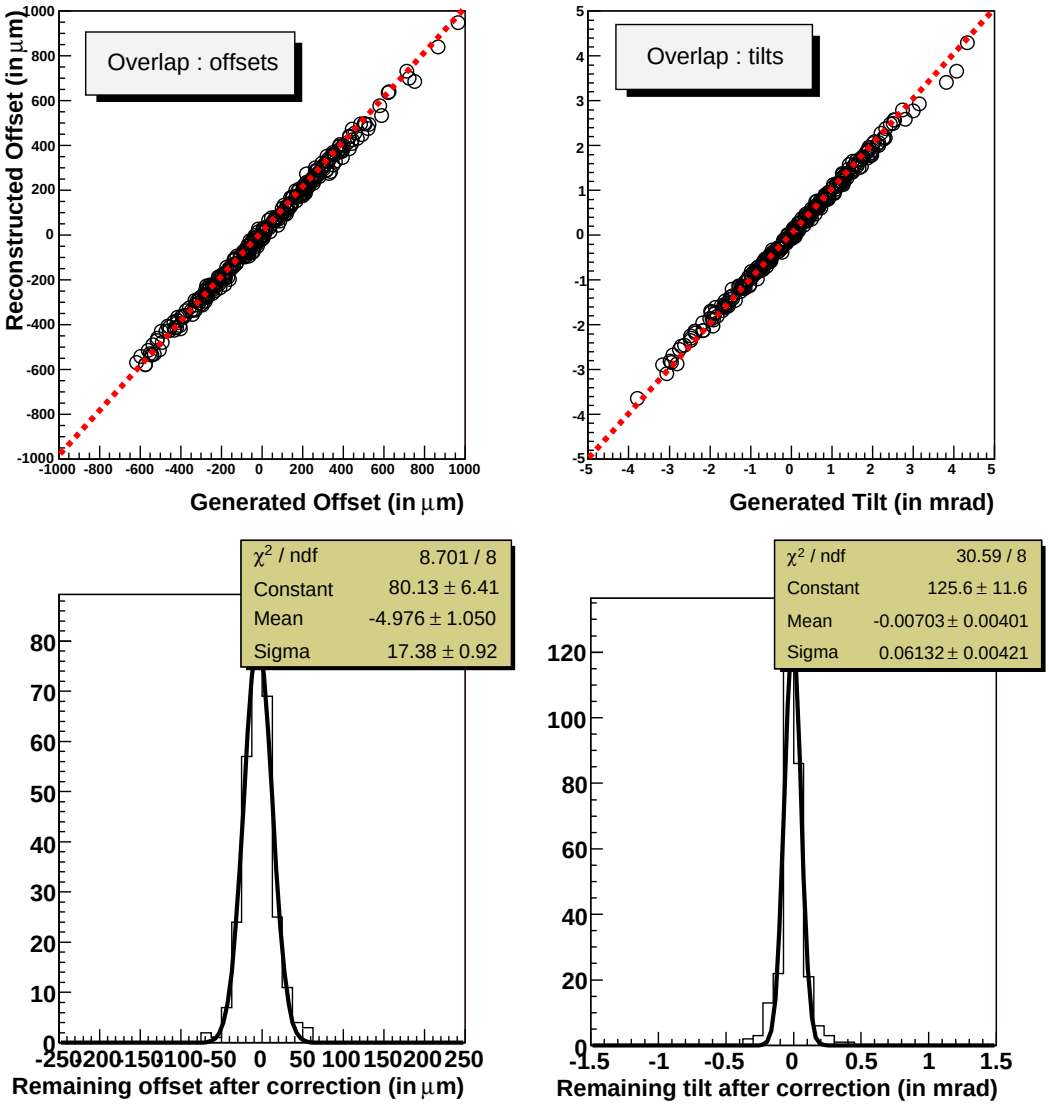

Figure 7 *Detector-half alignment with the overlapping tracks method and one detector half fixed. This gives the position of one detector-half w.r.t. the other. Top plots show the results obtained for detector-half offsets (Δ_x^B, Δ_y^B)(left) and tilts (Δ_α^B, Δ_β^B)(right). Bottom plots show the corresponding resolutions.*

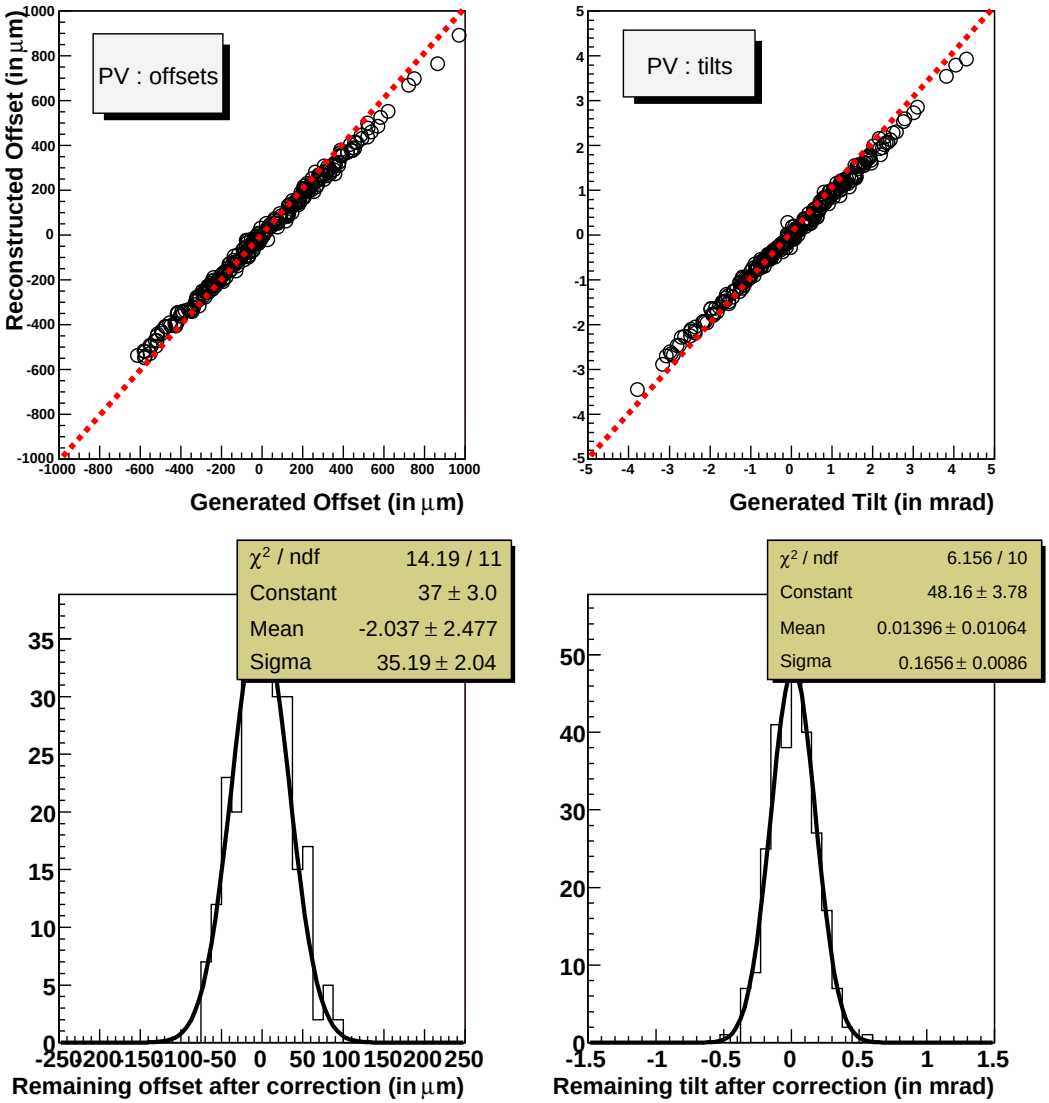

Figure 8 *Detector-half alignment with the primary vertices method only and one detector-half fixed. This gives the position of one detector-half w.r.t. the other. Top plots show the results obtained for detector-halves offsets (Δ_x^B, Δ_y^B)(left) and tilts (Δ_α^B, Δ_β^B)(right). Bottom plots show the corresponding resolutions.*

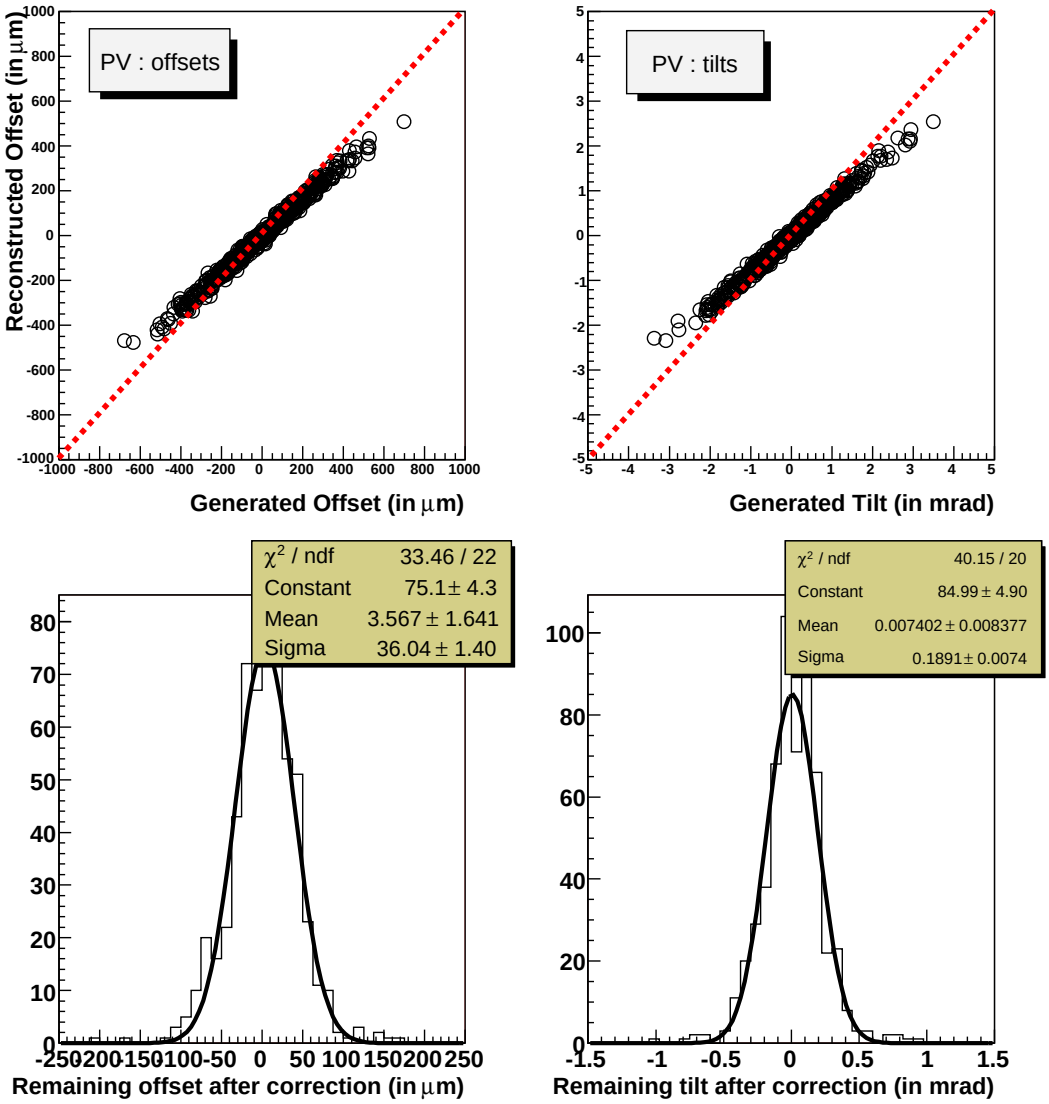

Figure 9 *Detector-half alignment with the primary vertices method only and vertex transverse position constrained. This gives the position of both detector-halves w.r.t. the beam. Top plots show the results obtained for detector-halves offsets ($\Delta_x^{B^{r,l}}$, $\Delta_y^{B^{r,l}}$)(left) and tilts ($\Delta_\alpha^{B^{r,l}}$, $\Delta_\beta^{B^{r,l}}$)(right). Bottom plots show the corresponding resolutions.*

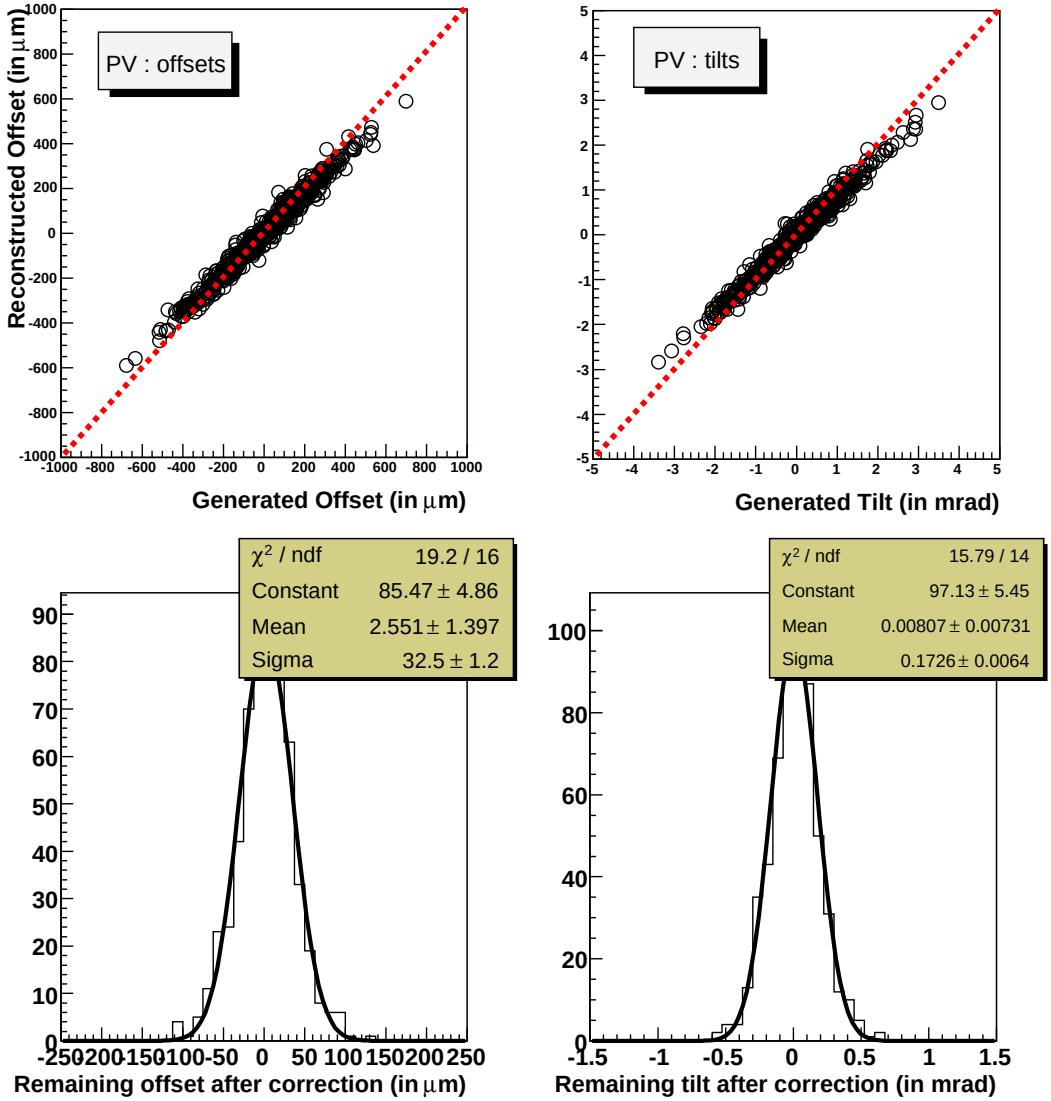

Figure 10 *Detector-half alignment with the primary vertices method and vertex transverse position constrained, adding the overlapping tracks method constraint. This gives the position of each detector-half independently w.r.t. the beam. Top plots show the results obtained for detector-halves offsets ($\Delta_x^{B^{r,l}}$, $\Delta_y^{B^{r,l}}$)(left) and tilts ($\Delta_\alpha^{B^{r,l}}$, $\Delta_\beta^{B^{r,l}}$)(right). Bottom plots show the corresponding resolutions.*

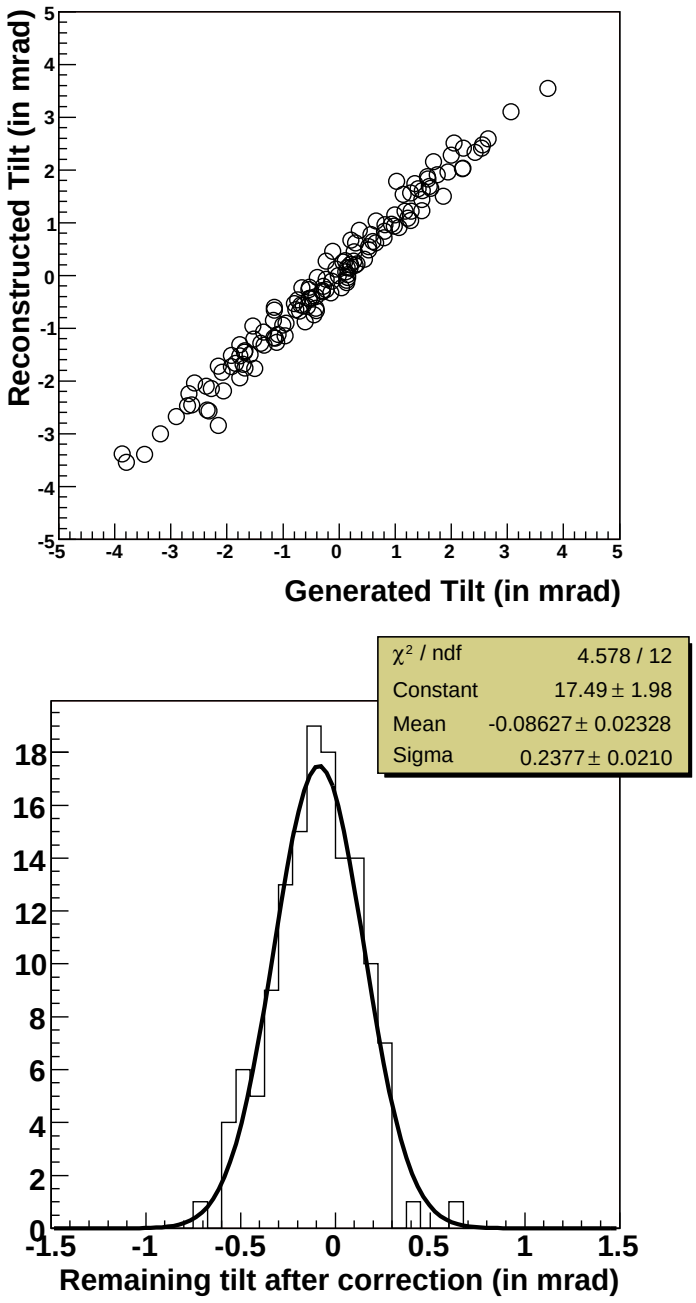

Figure 11 *Detector-half alignment with overlapping tracks. This give the position of one detector-half w.r.t. the other. Top plot shows the results obtained for detector-half Z tilt (Δ_γ^B). Bottom plot shows the corresponding resolution.*

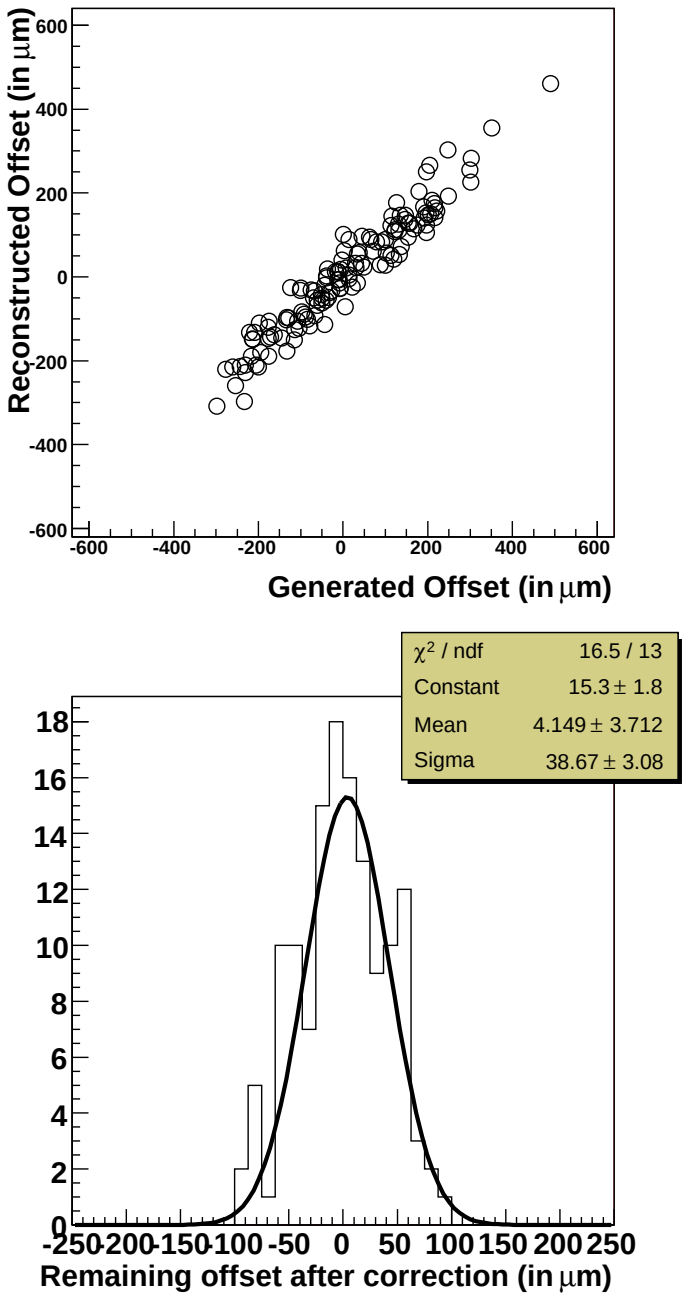

Figure 12 *Detector-half alignment with the primary vertices method only and one detector-half fixed. This give the position of one detector-half w.r.t. the other. Top plot shows the results obtained for detector-half Z offset (Δ_z^B). Bottom plot shows the corresponding resolution.*